

Electron slingshot acceleration in relativistic preturbulent shocks explored via emitted photon polarization

Zheng Gong,^{*} Xiaofei Shen, Karen Z. Hatsagortsyan,[†] and Christoph H. Keitel
Max-Planck-Institut für Kernphysik, Saupfercheckweg 1, 69117 Heidelberg, Germany

(Dated: July 4, 2023)

Electron acceleration mechanisms near the counterstreaming interface of a relativistic collisionless shock (RCS) are investigated using particle-in-cell (PIC) simulations. We identify a slingshot-like injection process induced by the drifting electric field sustained by the flowing focus of backwards-moving electrons, which is distinct from the well-known stochastic acceleration. The flowing focus signifies the plasma kinetic transition from a preturbulent laminar motion to a chaotic turbulence. We find a characteristic correlation between the electron dynamics in the slingshot acceleration and the photon emission features. In particular, the integrated radiation from the RCS exhibits a counterintuitive non-monotonic dependence of the photon polarization degree on the photon energy, which originates from a polarization degradation of relatively high-energy photons emitted by the slingshot-injected electrons. Our results demonstrate the potential of photon polarization as an essential information source in exploring intricate dynamics in RCSs with relevance for earth-based plasma and astrophysical scenarios.

Plasma shocks are characterized by rapid steepening of a nonlinear wave, the eventual overtaking by its rear part, and the irreversible energy transfer to the surrounding particles [1–3]. They are of extensive interest and ubiquitous in various scenarios, such as plasma accelerators [4–8], inertial confinement fusion [9–12], Earth’s magnetosphere bombarded by solar winds [13–15], young stellar outflows [16], and active galactic nuclei jets [17]. Recent observations suggest that RCSs offer plausible acceleration mechanisms towards understanding the origin of TeV cosmic leptons [18–21] and galactic PeVatrons [22]. Moreover, the unprecedented 100 TeV photon emission from the pulsar wind nebulae is interpreted as the Compton up-scattering of ultrarelativistic electrons driven by a RCS [23–25], and the RCS prompted afterglow radiation signals a peculiar long gamma-ray burst from the merger of a compact binary system [26–29].

The onset of filamentation turbulence in the RCS efficiently converts energy from ordered bulk flows to self-amplified fields [30–37]. This develops through the filamentation merging and magnetic loop coalescence [38–41], where electrons, undergoing turbulent motion with severe swirling and trace crossing, no longer travel in a quasi-layer form. The turbulence is crucial for characterizing Weibel-mediated microstructures [42–47] and instigating stochastic acceleration [48–54]. The latter, akin to the *Fermi* process [55, 56], refers to the particle energization through chaotic scatterings off inhomogeneous structures, which has been well recognized as sources of energetic electrons in RCSs [57–61]. Relevant experiments have testified the growth of magnetic filament turbulence [62–67] and the first-order Fermi acceleration [68]. However, it remains largely unexplored how the plasma transits from the nonturbulent flow to the kinetic turbulence and how this transition impacts the acceleration and radiation features in the RCS.

As a versatile information carrier of multi-messenger

astrophysics [69–71], photon polarization is critical for measuring the magnetic configuration nearby black holes [72] and crab nebulae [73] and for analyzing the particle acceleration in the blazar’s jet [74]. Therefore, the question arises whether the polarization feature of spontaneously emitted photons can be employed to reveal the mechanism responsible for the turbulence transition in a RCS.

In this letter, we investigate the electron dynamics in the transition to turbulence nearby the interface of a counterstreaming RCS. We employ PIC simulations to examine the photon emission and observe an anomalous non-monotonic dependence (NMD) of the photon polarization degree on the photon energy. We found that the NMD indicates a specific mechanism of electron acceleration, which we term as slingshot injection, caused by a drifting electric field due to the flowing focus of backwards-moving electrons. Utilizing Hamiltonian analyses, we elucidate that the backwards-flowing focus marks the plasma transition to a turbulent regime in the RCS, which in the electron’s transverse phase space is exhibited as the change from the phase-locked to the phase-slipping dynamics. The NMD photon properties stem from a polarization degradation of relatively high-energy photons emitted by the slingshot-injected electrons. The correlation among the NMD of photon polarization, the slingshot injection, and the backwards-flowing focus emphasizes the importance of the transition region to the turbulence in characterizing the acceleration and radiation in the RCS.

We have carried out 2D simulations of counterstreaming RCSs, see Fig. 1. The latter is initiated when a uniform plasma flow with a bulk Lorentz factor $\gamma_0 = 50$, injected from the right side, is reflected from the left side boundary, which adopts a reflection condition [58]. The periodic boundary condition is set in the lateral direction. Motivated by the unknown composition of as-

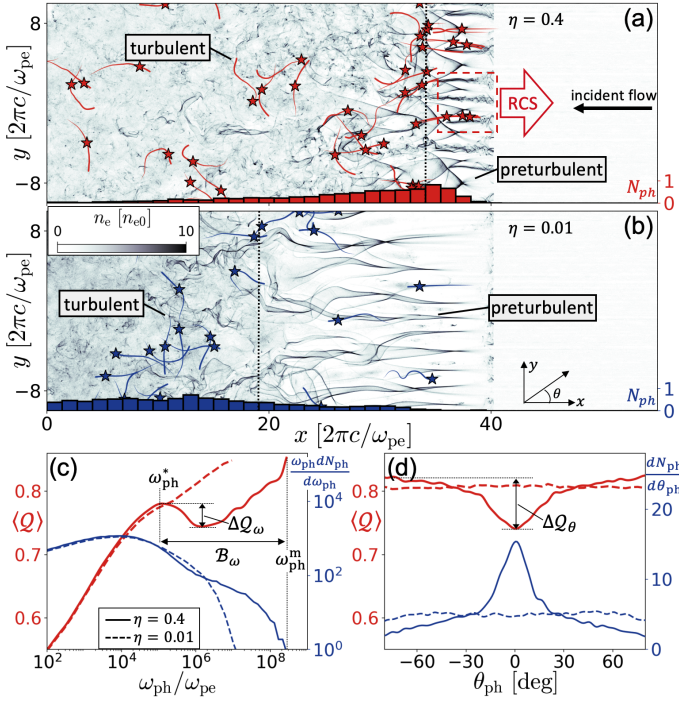


FIG. 1. The dynamics of a counterstreaming RCS: The electron density n_e at $t = 80\pi/\omega_{pe}$ for (a) $\eta = 0.4$ [75] and (b) $\eta = 0.01$ [76], where lines present the typical electron moving tendency with stars marking the photon emission and the histograms display the spatial distribution of emitted photons with $\omega_{ph} > 10^{-2}\omega_{ph}^m$. (c) $\langle Q \rangle$ and $\omega_{ph}dN_{ph}/d\omega_{ph}$ vs ω_{ph} . (d) $\langle Q \rangle$ and $dN_{ph}/d\theta_{ph}$ vs θ_{ph} .

trophysical jets, we consider the flow consisting of electrons, positrons, and ions with the number density of n_{e0} , n_{p0} , and n_{i0} , respectively. The charge neutralization $n_{e0} = n_{p0} + Z_i n_{i0}$ is satisfied initially and the ion with charge (mass) $Z_i = 1$ ($m_i = 1836m_e$) is used. The ratio $\eta \equiv n_{i0}/(n_{i0} + n_{p0}) \in (0.01, 1)$ denotes the proportion of ions among the whole positive charged particles. The simulation domain is $200\lambda_{pe} \times 20\lambda_{pe}$ with resolution $\Delta x = \Delta y = \lambda_{pe}/50$ and $\Delta t = 0.95\Delta x/c$. Each cell is filled with 48 macro-particles for each species. Here, $\omega_{pe} = (n_{e0}e^2/\varepsilon_0 m_e)^{1/2}$ ($\lambda_{pe} = 2\pi c/\omega_{pe}$) is the plasma frequency (skin depth), with the electron charge (mass) e (m_e), the vacuum permittivity ε_0 , and the speed of light c . The models of the photon polarization have been implemented in the EPOCH code [77, 78]. Unless otherwise indicated, we discuss results from the fiducial simulation with $\gamma_0 = 50$ and $\eta = 0.4$.

The snapshot of the electron density n_e in Fig. 1(a) exhibits that the filamentation exclusively exists at the front of the RCS interface. Between two adjacent filaments, an electron focusing point emerges, and following that, two oblique density strips stretch out [see Fig. 2(b)]. Behind the strips, the coherent filament structures and focusing points disappear while the turbulence shows up. A nontrivial thing is that the photons with energy $\varepsilon_{ph} \equiv \hbar\omega_{ph} > 10^{-2}\hbar\omega_{ph}^m$ are primarily emitted by elec-

trons nearby the interface, where $\omega_{ph}^m \sim 10^8\omega_{pe}$ is the photon cut-off frequency and \hbar the Planck constant. In contrast, in the case of $\eta = 0.01$, the energetic photon emission predominantly occurs in the turbulent region [see Fig. 1(b)], even though the preturbulent structures are extended to a larger range.

The degree of photon's linear polarization along the direction of the electron's transverse acceleration is characterized by the Stokes parameter Q [79], formulated as [78]

$$Q = \frac{\varepsilon_e(\varepsilon_e - \varepsilon_{ph})K_{\frac{2}{3}}(\zeta)}{[\varepsilon_e^2 + (\varepsilon_e - \varepsilon_{ph})^2]K_{\frac{2}{3}}(\zeta) - \varepsilon_e(\varepsilon_e - \varepsilon_{ph})\tilde{K}_{\frac{1}{3}}(\zeta)}, \quad (1)$$

where $K_n(\zeta)$ is the modified secondary Bessel function, $\tilde{K}_{1/3}(\zeta) = \int_{\zeta}^{\infty} K_{1/3}(z)dz$, $\zeta = 2\varepsilon_{ph}/[3\chi_e(\varepsilon_e - \varepsilon_{ph})]$, and $\varepsilon_e = \gamma_e m_e c^2$ the electron energy; $\chi_e \equiv (e\hbar/m_e^3 c^4)|F_{\mu\nu}p^\nu|$ is the electron quantum strong-field parameter with the field tensor $F_{\mu\nu}$, and the electron four-momentum p^ν . At $\chi_e \ll 0.1$, $\partial Q/\partial\varepsilon_{ph} > 0$ predicted by Eq. (1) manifests a monotonic dependence of Q on ω_{ph} , because for the higher-frequency radiation the formation length is shorter and the preservation of the local polarization degree is improved. This monotonic dependence is confirmed by the results of $\eta = 0.01$ [see Fig. 1(c)(d)], where electrons experience stochastic acceleration [48] and the photon emission is isotropic in the angular space. However, for $\eta = 0.4$ [see Fig. 1(c)(d)], the averaged polarization degree $\langle Q \rangle$ versus ω_{ph} exhibits NMD, with a polarization dip $\Delta Q_\omega \approx 4.5\%$ and a bandwidth ratio $\mathcal{B}_\omega \equiv \omega_{ph}^m/\omega_{ph}^* \sim 10^3$, contradictory to the forementioned monotonic dependence. Here, ω_{ph}^* is the local maximum point of the function $\langle Q \rangle$ vs ω_{ph} [see Fig. 1(c)]. In the angular distribution, $\langle Q \rangle$ has a polarization valley $\Delta Q_\theta \approx 11\%$ and the photon emission tends to be more collimated within an emission angle $\theta_{ph} \lesssim 15^\circ$.

To unveil the reason of the counterintuitive NMD, we focus on the electron dynamics within the dashed box marked in Fig. 1(a). For the deflection of backwards-moving electrons nearby the interface, the effective plasma density approximates ηn_{e0} and the charge density has a sinusoidal profile $\rho \sim |e|\eta n_{e0} \cos[k_y(y - y_c)]$ with $k_y \sim \omega_{pe}/2c$ the periodic wave number and y_c the relative central axis [78]. The self-generated transverse electric and magnetic field is calculated as $E_y(y) = (|e|\eta n_{e0}/\varepsilon_0 k_y) \sin[k_y(y - y_c)]$ and $B_z(y) = cE_y$. As justified by simulations, the energy exchange $d\gamma_e/dt$ is insignificant and thus the transverse dynamics is described by $\ddot{y} + (\Omega^2/k_y) \sin[k_y(y - y_c)] = 0$, with $\Omega^2 = 2\eta n_{e0} e^2/\varepsilon_0 \gamma_0 m_e$. Then the corresponding Hamiltonian can be derived as [78]

$$H_\perp(y, \dot{y}) = \frac{\Omega^2}{k_y^2} \cos[k_y(y - y_c)] + \frac{1}{2}\dot{y}^2. \quad (2)$$

Following $H_\perp(y, \dot{y}) = H_\perp(y_0, 0)$, the electron transverse

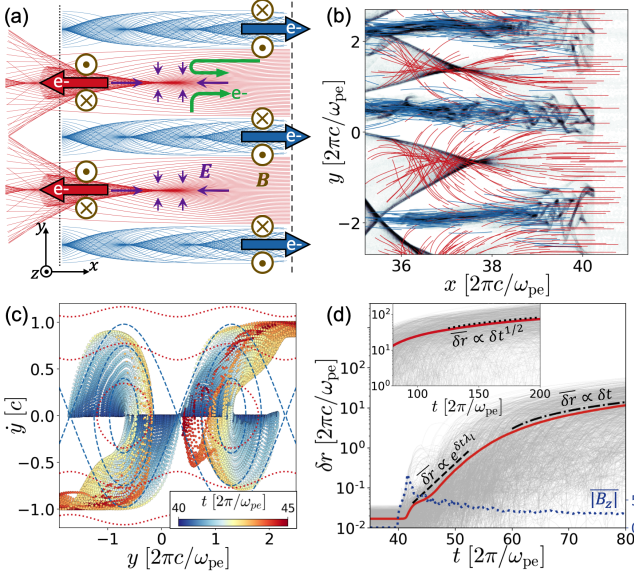


FIG. 2. (a) Schematic of the backwards-flowing focus with the predicted electron trajectories [80]. The brown (purple) markers denote the magnetic (electric) field direction and the green arrows present the slingshot-injected electrons. (b) Zoom in on the dashed box marked in Fig. 1(a), where the red (blue) lines represent the backward (forward) moving electrons [81]. (c) Electron evolution in (y, \dot{y}) space with the blue dashed (red dotted) lines contouring $H_{\perp}|_{\Omega \approx 0.1\omega_{pe}}$ ($H_{\perp}|_{\Omega' \approx 0.02\omega_{pe}}$) [82]. (d) Time evolution of δr ($\overline{\delta r}$) in grey (red).

motion is analyzed as

$$t = \frac{k_y}{\sqrt{2}\Omega} \int \frac{dy}{\sqrt{\cos[k_y(y_0 - y_c)] - \cos[k_y(y - y_c)]}}. \quad (3)$$

The trajectories predicted by Eq. (3) demonstrate that the backwards-moving electrons would be focused into $y = y_c$ at a restoring time $t_r \sim 0.6\pi/\Omega$, as confirmed by simulation results [see Figs. 2(a)(b)].

After the backwards-flowing focus, the electron motion starts to transit from the preturbulent motion to turbulence, interpreted as a shrinking of the Hamiltonian's separatrix. The separatrix $H_{\perp}(y, \dot{y}) \equiv H_{\perp}(y_c, 0) = \Omega^2/k_y^2$ divides the electron dynamics into the confined phase-locked and the escaping phase-slippage regions. If the magnetic field decreases with the equivalent restoring frequency reduced from Ω to Ω' , the phase space volume encompassed by the separatrix is shrunk from $H_{\perp}(y, \dot{y}) < \Omega^2/k_y^2$ to $H_{\perp}(y, \dot{y}) < \Omega'^2/k_y^2$. Thus, the electrons within the region of $\Omega'^2/k_y^2 < H_{\perp}(y, \dot{y}) < \Omega^2/k_y^2$ are released into the phase-slippage region [see Fig. 2(c)]. The electron release breaks the coherent filament structure and deteriorate the transverse inhomogeneity, leading to the onset of the plasma turbulence.

The transition from the preturbulent flowing focus to the turbulence is illustrated by the evolution of the particle separation [see Fig. 2(d)], where δr is the distance between an electron and its closest partner at the beginning and $\overline{\delta r}$ refers to the averaged value. After the

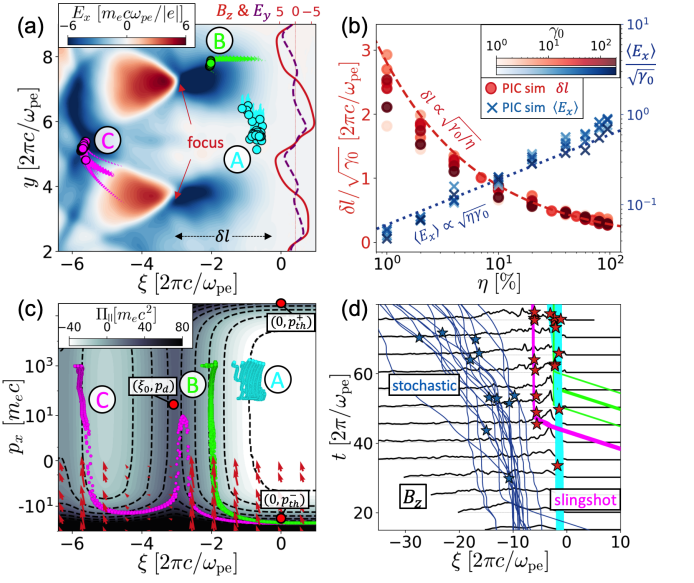


FIG. 3. (a) Electric field E_x with the transverse profile of B_z and E_y . (b) δl and $\langle E_x \rangle$ vs η . (c) Hamiltonian $\Pi_{\parallel}(\xi, p_x)$ with the red arrows denoting the moving tendency modified by the magnetic deflection. (d) Time-evolved electron position, where the black lines profile B_z and the red (blue) stars mark the photon emission belong to the slingshot (stochastic) mechanism. Three kinds of slingshot electrons are shown with the color of 'A' cyan, 'B' lime, and 'C' magenta.

focus at $\omega_{pe}t/2\pi \sim 45$, the signature of the chaotic dynamics arises with $\overline{\delta r} \propto \exp(\lambda_l \delta t)$ characterized by the Lyapunov exponent $\lambda_l \approx 0.15\omega_{pe}/\pi$ [83]. The electrons exhibit a chaotic behavior during the defocusing stage [84], where the decrease of the exerted magnetic field $|B_z|$ proves the shrinking of the Hamiltonian's separatrix. Later at $\omega_{pe}t/2\pi \sim 70$, $\overline{\delta r} \propto 0.2\epsilon\delta t/\pi$ implies a drifting tendency because of the localized electrons prone to occupy the whole interaction domain [85]. Eventually at $\omega_{pe}t/2\pi > 130$, $\overline{\delta r} \propto 9(\omega_{pe}\delta t/2\pi)^{1/2}$ manifests the electrons' random walk procedure [86, 87].

The flowing focus leads to a negative longitudinal electric field E_x with a scale length δl [see Fig. 3(a)], favorable for injecting electrons into the RCS. This injection resembles a slingshot, where the filaments serve as the handhold, the backwards-moving electrons behave as the elastic string, and the injected forwards-moving electrons are the projectiles [88]. The scale length is calculated as $\delta l \sim t_r c \approx \pi\sqrt{\gamma_0/\eta}(c/\omega_{pe})$. Given $\nabla \cdot \mathbf{E} = \rho/\epsilon_0$, the field strength is estimated as $\langle E_x \rangle \approx \pi\sqrt{\eta\gamma_0}m_e c\omega_{pe}/|e|$ [see Fig. 3(b)]. The flowing focus successively occurs for the replenished backwards-moving electrons and the field E_x propagates with a velocity $v_x \approx v_d = (1 - 1/\gamma_0^2)^{1/2}$. In the interface's co-moving frame $\xi = x - v_d t$, the electron's longitudinal dynamics is determined by the Hamiltonian $\Pi_{\parallel}(\xi, p_x) = -|e|\varphi(\xi) + c\sqrt{m_e^2 c^2 + p_x^2} - v_d p_x$ with $\varphi(\xi) = -\int E_x(\xi)d\xi$ [see Fig. 3(c)] [78]. Considering the separatrix (ξ_0, p_d) with $E_x(\xi_0) = 0$ and $p_d = m_e v_d/(1 - v_d^2/c^2)^{1/2}$, the relation $\Pi_{\parallel}(0, p_{th}^{\pm}) = \Pi_{\parallel}(\xi_0, p_d)$

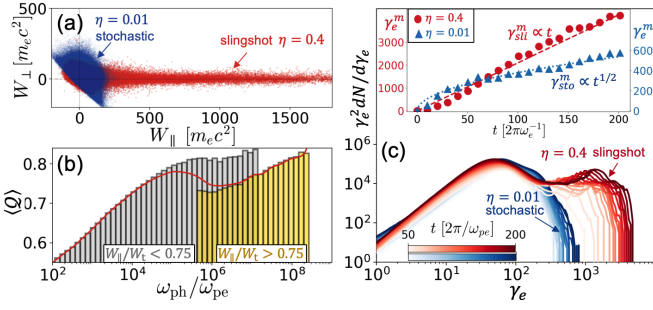


FIG. 4. (a) Distribution of W_{\perp} at the emission moment. (b) $\langle Q \rangle$ vs ω_{ph} for photons associated with $W_{\parallel}/W_t \leq 0.75$, where the red line reproduces the $\langle Q \rangle$ vs ω_{ph} in Fig. 1(c). (c) Time-evolved electron energy spectral $\gamma_e^2 dN/d\gamma_e$. The inset displays the time-dependent electron maximum energy γ_e^m .

governs the injection threshold p_{th}^- and the maximum achievable momentum p_{th}^+ , derived as [78]

$$p_{th}^+ \sim 2\gamma_0^3 + \frac{3}{2}\gamma_0 - \frac{2}{\gamma_0} \quad \& \quad p_{th}^- \sim -\frac{\gamma_0}{2} - \frac{1}{2\gamma_0}. \quad (4)$$

Specifically, there are three types of slingshot-injected electrons [see Figs. 3] [89]. The ‘A’ electrons co-moving with E_x get a pronounced energy gain up to $\gamma_e \sim 10^3$ for the considered parameters. The initially backwards-moving ‘B’ electrons are below the threshold, i.e. $p_x \sim -\gamma_0 < p_{th}^-$, but they are still injected because the magnetic deflection $\mathbf{v} \times \mathbf{B}$ leading to an attractor effect in (ξ, p_x) space [90, 91], which drags the electrons towards the degraded Hamiltonian Π_{\parallel} [see the red arrows in Fig. 3(c)] [78]. The ‘C’ electrons are trapped by the E_x induced by assembling two stretched-out density strips behind the flowing focus position. Unlike the directed slingshot electrons, the stochastic electrons tend to be repetitively rebounded by the magnetic turbulence and undergo Fermi-like acceleration [58, 59]. Figure 3(d) manifests that the primary contribution of photon emission nearby the preturbulent RCS interface originates from the slingshot electrons.

In the search for a distinct criterion distinguishing between the slingshot and stochastic electrons, we turn to the electron’s longitudinal and transverse work $W_{\parallel, \perp}$ [see Fig. 4(a)], where $W_{\parallel} = -\int |e|E_x dx$, $W_{\perp} = -\int |e|E_y dy$, and $W_t = W_{\parallel} + W_{\perp}$; the integrals are calculated from the beginning to the photon emitting moment. The slingshot acceleration relies on E_x while the stochastic process is isotropic, meaning that the photon emission associated with $W_{\parallel}/W_t \rightarrow 1$ ($W_{\parallel}/W_t \rightarrow 0.5$) belong to the slingshot (stochastic) mechanism [92]. Therefore, the condition of $W_{\parallel}/W_t \leq 0.75$ is a reasonable criterion to distinguish the photon emission from the stochastic or slingshot mechanism. For the photons produced from the two mechanisms, both of their $\langle Q \rangle$ vs ω_{ph} [in Fig. 4(b)] is monotonically increasing as predicted by Eq.(1). However, the photon emission from the slingshot is shifted to the higher frequency range compared with the stochastic scenario due to the enhanced energy of slingshot electrons

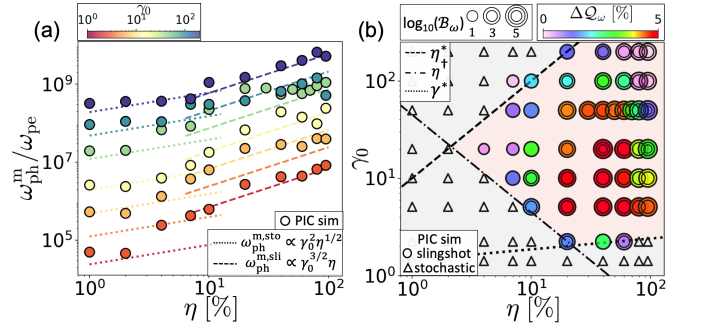


FIG. 5. (a) ω_{ph}^m vs η . (b) Dependence of ΔQ_{ω} and \mathcal{B}_{ω} on η and γ_0 , where the circles (triangles) refer to the electron dynamics dominated by the slingshot (stochastic) mechanism.

[see Fig. 4(c)]. Therefore, the NMD of $\langle Q \rangle$ vs ω_{ph} comes from the combination between the high polarization degree stochastic photons and the low polarization degree slingshot photons around $\omega_{ph} \sim 10^6 \omega_{pe}$ [see Fig. 4(b)]. Nearby this frequency region, the emission of both mechanisms contributes.

The maximum slingshot energy γ_{sli}^m is approximated as $\gamma_{sli}^m \sim |e| \langle E_x \rangle \delta t / m_e c \sim \pi \sqrt{\eta \gamma_0} \omega_{pe} \delta t$ when the electron energy is far from the saturation $\gamma_e \ll p_{th}^+ \sim 10^6$. The energy gain of the stochastic process is estimated using the random walk model [86]: $\gamma_{sto}^m \sim 0.5(\omega_{pe,0} \delta t)^{1/2} \gamma_0^{3/4} \eta^{1/4}$ [78]. These estimates agree well with the simulation results [Fig. 4(c)]. Following γ_{sli}^m and γ_{sto}^m , the photon cut-off frequency ω_{ph}^m for the slingshot and stochastic mechanisms is predicted as $\omega_{ph}^{m, sli} \sim \gamma_{sli}^{m2} B \propto \gamma_0^{3/2} \eta$ and $\omega_{ph}^{m, sto} \sim \gamma_{sto}^{m2} B \propto \gamma_0^2 \eta^{1/2}$ [see Fig. 5(a)] with the magnetic field strength $B \propto \gamma_0^{1/2}$.

Examining the NMD polarization features of the polarization dip ΔQ_{ω} and the bandwidth \mathcal{B}_{ω} , we conclude that the high-frequency photon emission is dominated by the slingshot mechanism due to fulfilling three criteria: i) the photon cut-off frequency originating from slingshot electrons is much higher than via the stochastic mechanism, i.e. $\omega_{ph}^{m, sli} \gg \omega_{ph}^{m, sto}$, reformulated as $\eta \gtrsim \eta^* = 0.01\gamma_0$; ii) the number of the slingshot injected electron $N_e^{sli} \propto \langle E_x \rangle$ should be larger than the most energetic part of the stochastic electrons $N_e^{sto} \propto n_{pe0}$, rearranged as $\eta \gtrsim \eta^{\dagger} \propto \gamma_0^{-1}$; iii) the saturation of the slingshot acceleration should be higher than the stochastic acceleration, i.e. $p_{th}^+ \gtrsim \gamma_{sto}^m$, expressed as $\gamma_0 \gtrsim \gamma^* = 2\eta^{1/9}$. The criteria of the slingshot dominance predicted by $\eta > \max\{\eta^*, \eta^{\dagger}\}$ and $\gamma > \gamma^*$ agrees well with the simulation results [see Fig. 5(b)]. The dependence of ΔQ_{ω} and \mathcal{B}_{ω} on η and γ_0 in Fig. 5(b) confirms that the NMD of the polarization degree on photon energy is exclusively from the emission dominated by the slingshot mechanism.

In conclusion, inspecting the origin of unexpected polarization features of the photon radiation in the preturbulent RCS, we have identified the electron slingshot-like acceleration mechanism, distinct from the known

stochastic process [48–54]. The slingshot injection is induced by the electron backwards-flowing focus associated with the transition to turbulence in the RCS’s counterstreaming interface. The identified features of the transition region to turbulence, slingshot injection, and photon polarization dependence have crucial implications for both laboratory and astrophysical phenomena. For instance, the turbulence transition with the backwards-flowing focus may deteriorate the ignition efficiency in confinement fusion by yielding superthermal particles nearby the interface of a beam propagating in dense plasmas [93–95]. Moreover, the slingshot procedure provides an alternative mechanism accounting for TeV cosmic electrons [19] and feasible pre-stage injection for the subsequent infinite *Fermi* acceleration in RCSs [96]. Finally, the nontrivial photon polarization dynamics suggests the necessity of revising the retrieval procedure for astrophysical magnetic configuration based on the radiation features [72, 73, 97, 98].

The original version of code EPOCH adapted here is funded by the UK EPSRC grants EP/G054950/1, EP/G056803/1, EP/G055165/1 and EP/ M022463/1. The authors would like to thank Laurent Gremillet, Anatoly Spitkovsky, and Dmitri Uzdensky for the discussion regarding plasma stream instabilities, the initialization of RCS in PIC simulations, and the undetermined composition of astrophysical jets, respectively. Z. G. also thanks Zhi-Qiu Huang for the gained knowledge about the RCS generated following gamma-ray bursts.

* gong@mpi-hd.mpg.de

† k.hatsagortsyan@mpi-hd.mpg.de

- [1] R. Sagdeev, Cooperative phenomena and shock waves in collisionless plasmas, *Reviews of plasma physics* **4**, 23 (1966).
- [2] R. Courant and K. O. Friedrichs, *Supersonic flow and shock waves*, Springer Science & Business Media **21** (1999).
- [3] L. D. Landau and E. M. Lifshitz, *Fluid mechanics: Course of theoretical physics*, volume 6, **6** (2013).
- [4] L. O. Silva, M. Marti, J. R. Davies, R. A. Fonseca, C. Ren, F. S. Tsung, and W. B. Mori, Proton shock acceleration in laser-plasma interactions, *Physical Review Letters* **92**, 015002 (2004).
- [5] F. Fiúza, A. Stockem, E. Boella, R. Fonseca, L. Silva, D. Haberberger, S. Tochitsky, C. Gong, W. B. Mori, and C. Joshi, Laser-driven shock acceleration of monoenergetic ion beams, *Physical Review Letters* **109**, 215001 (2012).
- [6] D. Haberberger, S. Tochitsky, F. Fiúza, C. Gong, R. A. Fonseca, L. O. Silva, W. B. Mori, and C. Joshi, Collisionless shocks in laser-produced plasma generate monoenergetic high-energy proton beams, *Nature Physics* **8**, 95 (2012).
- [7] H. Zhang, B. Shen, W. Wang, *et al.*, Collisionless shock acceleration of high-flux quasimonoenergetic proton beams driven by circularly polarized laser pulses, *Physical review letters* **119**, 164801 (2017).
- [8] Y. Yao *et al.*, High-flux neutron generator based on laser-driven collisionless shock acceleration, *Physical Review Letters*, accepted 24 May (2023).
- [9] R. Betti, C. Zhou, K. Anderson, L. Perkins, W. Theobald, and A. Solodov, Shock ignition of thermonuclear fuel with high areal density, *Physical review letters* **98**, 155001 (2007).
- [10] L. J. Perkins, R. Betti, K. LaFortune, and W. Williams, Shock ignition: A new approach to high gain inertial confinement fusion on the national ignition facility, *Physical review letters* **103**, 045004 (2009).
- [11] C. Riconda, S. Weber, V. Tikhonchuk, and A. Héron, Kinetic simulations of stimulated raman backscattering and related processes for the shock-ignition approach to inertial confinement fusion, *Physics of Plasmas* **18**, 092701 (2011).
- [12] R. Scott, D. Barlow, W. Trickey, A. Ruocco, K. Glize, L. Antonelli, M. Khan, and N. Woolsey, Shock-augmented ignition approach to laser inertial fusion, *Physical Review Letters* **129**, 195001 (2022).
- [13] D. Turner, L. Wilson III, T. Liu, I. Cohen, S. Schwartz, A. Osmane, J. Fennell, J. Clemmons, J. Blake, J. Westlake, *et al.*, Autogenous and efficient acceleration of energetic ions upstream of earth’s bow shock, *Nature* **561**, 206 (2018).
- [14] T. Amano, T. Katou, N. Kitamura, M. Oka, Y. Matsumoto, M. Hoshino, Y. Saito, S. Yokota, B. Giles, W. Paterson, *et al.*, Observational evidence for stochastic shock drift acceleration of electrons at the earth’s bow shock, *Physical review letters* **124**, 065101 (2020).
- [15] L. Turc, O. W. Roberts, D. Verscharen, A. P. Dimmock, P. Kajdič, M. Palmroth, Y. Pfau-Kempf, A. Johlander, M. Dubart, E. Kilpua, *et al.*, Transmission of foreshock waves through earth’s bow shock, *Nature Physics*, 1 (2022).
- [16] B. Reipurth and J. Bally, Herbig-haro flows: Probes of early stellar evolution, *Annual Review of Astronomy and Astrophysics* **39**, 403 (2001).
- [17] R. Blandford, D. Meier, and A. Readhead, Relativistic jets from active galactic nuclei, *Annual Review of Astronomy and Astrophysics* **57**, 467 (2019).
- [18] M. Aguilar, L. A. Cavazonza, G. Ambrosi, L. Arruda, N. Attig, *et al.*, Towards understanding the origin of cosmic-ray positrons, *Physical review letters* **122**, 041102 (2019).
- [19] M. Aguilar, L. A. Cavazonza, B. Alpat, G. Ambrosi, L. Arruda, A. Barrau, *et al.*, Towards understanding the origin of cosmic-ray electrons, *Physical review letters* **122**, 101101 (2019).
- [20] R. Dising and D. Caprioli, Spectrum of electrons accelerated in supernova remnants, *Physical Review Letters* **123**, 071101 (2019).
- [21] K. Koyama, R. Petre, E. Gotthelf, U. Hwang, M. Matsuura, M. Ozaki, and S. Holt, Evidence for shock acceleration of high-energy electrons in the supernova remnant sn1006, *Nature* **378**, 255 (1995).
- [22] K. Fang, M. Kerr, R. Blandford, H. Fleischhack, and E. Charles, Evidence for pev proton acceleration from fermi-lat observations of snr g 106.3+ 2.7, *Physical Review Letters* **129**, 071101 (2022).
- [23] M. Amenomori *et al.*, First detection of photons with energy beyond 100 tev from an astrophysical source,

- Physical review letters **123**, 051101 (2019).
- [24] M. Amenomori *et al.*, Gamma-ray observation of the cygnus region in the 100-tev energy region, Physical Review Letters **127**, 031102 (2021).
- [25] H. Collaboration, Resolving the crab pulsar wind nebula at teraelectronvolt energies, Nature astronomy **4**, 167 (2020).
- [26] E. Troja *et al.*, A nearby long gamma-ray burst from a merger of compact objects, Nature **612**, 228 (2022).
- [27] J. C. Rastinejad, N. R. Tanvir, *et al.*, A kilonova following a long-duration gamma-ray burst at 350 mpc, Nature **612**, 223 (2022).
- [28] A. Mei, B. Banerjee, G. Oganessian, *et al.*, Giga-electronvolt emission from a compact binary merger, Nature **612**, 236 (2022).
- [29] J. Yang *et al.*, A long-duration gamma-ray burst with a peculiar origin, Nature **612**, 232 (2022).
- [30] M. V. Medvedev and A. Loeb, Generation of magnetic fields in the relativistic shock of gamma-ray burst sources, The Astrophysical Journal **526**, 697 (1999).
- [31] L. Silva, R. Fonseca, J. Tonge, J. Dawson, W. Mori, and M. Medvedev, Interpenetrating plasma shells: near-equipartition magnetic field generation and nonthermal particle acceleration, The Astrophysical Journal **596**, L121 (2003).
- [32] A. Bell, Turbulent amplification of magnetic field and diffusive shock acceleration of cosmic rays, Monthly Notices of the Royal Astronomical Society **353**, 550 (2004).
- [33] A. Bret, M.-C. Firpo, and C. Deutsch, Characterization of the initial filamentation of a relativistic electron beam passing through a plasma, Physical review letters **94**, 115002 (2005).
- [34] F. Califano, D. Del Sarto, and F. Pegoraro, Three-dimensional magnetic structures generated by the development of the filamentation (weibel) instability in the relativistic regime, Physical review letters **96**, 105008 (2006).
- [35] A. Bret, L. Gremillet, D. Bénisti, and E. Lefebvre, Exact relativistic kinetic theory of an electron-beam-plasma system: Hierarchy of the competing modes in the system-parameter space, Physical review letters **100**, 205008 (2008).
- [36] A. Marcowith, A. Bret, A. Bykov, M. E. Dieckman, L. O. Drury, B. Lembège, M. Lemoine, G. Morlino, G. Murphy, G. Pelletier, *et al.*, The microphysics of collisionless shock waves, Reports on Progress in Physics **79**, 046901 (2016).
- [37] A. Grassi, M. Grech, F. Amiranoff, A. Macchi, and C. Riconda, Radiation-pressure-driven ion weibel instability and collisionless shocks, Physical Review E **96**, 033204 (2017).
- [38] F. Califano, N. Attico, F. Pegoraro, G. Bertin, and S. Bulanov, Fast formation of magnetic islands in a plasma in the presence of counterstreaming electrons, Physical review letters **86**, 5293 (2001).
- [39] M. Honda, J. Meyer-ter Vehn, and A. Pukhov, Collective stopping and ion heating in relativistic-electron-beam transport for fast ignition, Physical review letters **85**, 2128 (2000).
- [40] J. R. Peterson, S. Glenzer, and F. Fiuza, Magnetic field amplification by a nonlinear electron streaming instability, Physical Review Letters **126**, 215101 (2021).
- [41] Z. Gong, K. Z. Hatsagortsyan, and C. H. Keitel, Electron polarization in ultrarelativistic plasma current filamentation instabilities, Physical Review Letters **130**, 015101 (2023).
- [42] E. S. Weibel, Spontaneously growing transverse waves in a plasma due to an anisotropic velocity distribution, Physical Review Letters **2**, 83 (1959).
- [43] F. Fiuza, R. Fonseca, J. Tonge, W. B. Mori, and L. Silva, Weibel-instability-mediated collisionless shocks in the laboratory with ultraintense lasers, Physical Review Letters **108**, 235004 (2012).
- [44] C. Ruyer, L. Gremillet, G. Bonnaud, and C. Riconda, Analytical predictions of field and plasma dynamics during nonlinear weibel-mediated flow collisions, Physical Review Letters **117**, 065001 (2016).
- [45] V. Zhdankin, G. R. Werner, D. A. Uzdensky, and M. C. Begelman, Kinetic turbulence in relativistic plasma: from thermal bath to nonthermal continuum, Physical Review Letters **118**, 055103 (2017).
- [46] M. Lemoine, L. Gremillet, G. Pelletier, and A. Vanthieghem, Physics of weibel-mediated relativistic collisionless shocks, Physical review letters **123**, 035101 (2019).
- [47] A. Bohdan, M. Pohl, J. Niemiec, P. J. Morris, Y. Matsumoto, T. Amano, M. Hoshino, and A. Sulaiman, Magnetic field amplification by the weibel instability at planetary and astrophysical shocks with high mach number, Phys. Rev. Lett. **126**, 095101 (2021).
- [48] V. Petrosian, Stochastic acceleration by turbulence, Space science reviews **173**, 535 (2012).
- [49] M. Hoshino, Stochastic particle acceleration in multiple magnetic islands during reconnection, Physical Review Letters **108**, 135003 (2012).
- [50] Y. Matsumoto, T. Amano, T. N. Kato, and M. Hoshino, Electron surfing and drift accelerations in a weibel-dominated high-mach-number shock, Physical review letters **119**, 105101 (2017).
- [51] L. Comisso and L. Sironi, Particle acceleration in relativistic plasma turbulence, Physical review letters **121**, 255101 (2018).
- [52] V. Zhdankin, D. A. Uzdensky, G. R. Werner, and M. C. Begelman, Electron and ion energization in relativistic plasma turbulence, Physical review letters **122**, 055101 (2019).
- [53] L. Comisso and L. Sironi, Pitch-angle anisotropy controls particle acceleration and cooling in radiative relativistic plasma turbulence, Physical Review Letters **127**, 255102 (2021).
- [54] M. Lemoine, First-principles fermi acceleration in magnetized turbulence, Physical Review Letters **129**, 215101 (2022).
- [55] E. Fermi, On the origin of the cosmic radiation, Physical review **75**, 1169 (1949).
- [56] E. Fermi, Galactic magnetic fields and the origin of cosmic radiation., The Astrophysical Journal **119**, 1 (1954).
- [57] A. Bell, The acceleration of cosmic rays in shock fronts—i, Monthly Notices of the Royal Astronomical Society **182**, 147 (1978).
- [58] A. Spitkovsky, Particle acceleration in relativistic collisionless shocks: Fermi process at last?, The Astrophysical Journal **682**, L5 (2008).
- [59] Y. Matsumoto, T. Amano, T. Kato, and M. Hoshino, Stochastic electron acceleration during spontaneous turbulent reconnection in a strong shock wave, Science **347**, 974 (2015).

- [60] L. Sironi, U. Keshet, and M. Lemoine, Relativistic shocks: particle acceleration and magnetization, *Space Science Reviews* **191**, 519 (2015).
- [61] T. Amano, Y. Matsumoto, A. Bohdan, O. Kobzar, S. Matsukiyo, M. Oka, J. Niemiec, M. Pohl, and M. Hoshino, Nonthermal electron acceleration at collisionless quasi-perpendicular shocks, *Reviews of Modern Plasma Physics* **6**, 29 (2022).
- [62] G. Gregori, A. Ravasio, C. Murphy, K. Schaar, A. Baird, A. Bell, A. Benuzzi-Mounaix, R. Bingham, C. Constantin, R. Drake, *et al.*, Generation of scaled protogalactic seed magnetic fields in laser-produced shock waves, *Nature* **481**, 480 (2012).
- [63] N. Kugland, D. Ryutov, P. Chang, R. Drake, G. Fiksel, D. Froula, S. Glenzer, G. Gregori, M. Grosskopf, M. Koenig, *et al.*, Self-organized electromagnetic field structures in laser-produced counter-streaming plasmas, *Nature Physics* **8**, 809 (2012).
- [64] W. Fox, G. Fiksel, A. Bhattacharjee, P.-Y. Chang, K. Germaschewski, S. Hu, and P. Nilson, Filamentation instability of counterstreaming laser-driven plasmas, *Physical review letters* **111**, 225002 (2013).
- [65] C. Huntington, F. Fiuza, J. Ross, A. Zylstra, R. Drake, D. Froula, G. Gregori, N. Kugland, C. Kuranz, M. Levy, *et al.*, Observation of magnetic field generation via the weibel instability in interpenetrating plasma flows, *Nature Physics* **11**, 173 (2015).
- [66] C. Li, V. Tikhonchuk, Q. Moreno, H. Sio, E. d’Humières, X. Ribeyre, P. Korneev, S. Atzeni, R. Betti, A. Birkel, *et al.*, Collisionless shocks driven by supersonic plasma flows with self-generated magnetic fields, *Physical review letters* **123**, 055002 (2019).
- [67] C. Ruyer, S. Bolaños, B. Albertazzi, S. Chen, P. Antici, J. Böker, V. Dervieux, L. Lancia, M. Nakatsutsumi, L. Romagnani, *et al.*, Growth of concomitant laser-driven collisionless and resistive electron filamentation instabilities over large spatiotemporal scales, *Nature Physics* **16**, 983 (2020).
- [68] F. Fiuza, G. Swadling, A. Grassi, H. Rinderknecht, D. Higginson, D. Ryutov, C. Bruulsema, R. Drake, S. Funk, S. Glenzer, *et al.*, Electron acceleration in laboratory-produced turbulent collisionless shocks, *Nature physics* **16**, 916 (2020).
- [69] I. Bartos and M. Kowalski, *Multimessenger* (IOP Publishing Bristol, 2017).
- [70] P. Mészáros, D. B. Fox, C. Hanna, and K. Murase, Multi-messenger astrophysics, *Nature Reviews Physics* **1**, 585 (2019).
- [71] E. Komatsu, New physics from the polarized light of the cosmic microwave background, *Nature Reviews Physics* **4**, 452 (2022).
- [72] K. Akiyama, J. C. Algaba, A. Alberdi, W. Alef, R. Anantua, K. Asada, R. Azulay, A.-K. Baczkó, D. Ball, M. Baloković, *et al.*, First m87 event horizon telescope results. viii. magnetic field structure near the event horizon, *The Astrophysical Journal Letters* **910**, L13 (2021).
- [73] N. Bucciantini, R. Ferrazzoli, M. Bachetti, J. Rankin, N. Di Lalla, C. Sgrò, N. Omodei, T. Kitaguchi, T. Mizuno, S. Gunji, *et al.*, Simultaneous space and phase resolved x-ray polarimetry of the crab pulsar and nebula, *Nature Astronomy* , 1 (2023).
- [74] I. Liodakis, A. P. Marscher, I. Agudo, A. V. Berdyugin, M. I. Bernardos, G. Bonnoli, G. A. Borman, C. Casadio, V. Casanova, E. Cavazzuti, *et al.*, Polarized blazar x-rays imply particle acceleration in shocks, *Nature* **611**, 677 (2022).
- [75] See the animation for the detailed electron density, electron motion, and photon emission for the case of $\eta = 0.4$ (animation_fig1a_density_eta040.gif).
- [76] See the animation for the detailed electron density, electron motion, and photon emission for the case of $\eta = 0.01$ (animation_fig1a_density_eta001.gif).
- [77] T. Arber, K. Bennett, C. Brady, A. Lawrence-Douglas, M. Ramsay, N. Sircombe, P. Gillies, R. Evans, H. Schmitz, A. Bell, *et al.*, Contemporary particle-in-cell approach to laser-plasma modelling, *Plasma Physics and Controlled Fusion* **57**, 113001 (2015).
- [78] See the Supplemental Materials for the discussion on the model of photon polarization implemented in PIC code, the analytical derivation for electron dynamics in backwards-flowing focus and slingshot injection, and the electron stochastic acceleration based on the random walk model. The Supplemental Materials include Ref. [99–104].
- [79] W. H. McMaster, Polarization and the stokes parameters, *American Journal of Physics* **22**, 351 (1954).
- [80] See the animation for the analytically predicted electron trajectories of the backwards-flowing focus (animation_fig2a.gif).
- [81] See the animation for the simulated electron trajectories of the backwards-flowing focus (animation_fig2b.gif).
- [82] See the animation for the analytically predicted electron evolution in the transverse phase space (animation_fig2c_analytical.gif).
- [83] A. Vulpiani, F. Cecconi, and M. Cencini, *Chaos: from simple models to complex systems*, Vol. 17 (World Scientific, 2009).
- [84] See the animation for the detailed evolution of δr and electron motion at $\omega_{pe}t/2\pi \sim 45$. (animation_fig2d_1.gif).
- [85] See the animation for the detailed evolution of δr and electron motion at $\omega_{pe}t/2\pi \sim 70$. (animation_fig2d_2.gif).
- [86] O. C. Ibe, *Elements of random walk and diffusion processes* (John Wiley & Sons, 2013).
- [87] See the animation for the detailed evolution of δr and electron motion at $\omega_{pe}t/2\pi > 130$. (animation_fig2d_3.gif).
- [88] See the animation for the detailed electron dynamics and photon emission (animation_shining_eta040.gif).
- [89] See the animation for the detailed slingshot injection process (animation_fig3a.gif).
- [90] M. W. Hirsch, S. Smale, and R. L. Devaney, *Differential equations, dynamical systems, and an introduction to chaos* (Academic press, 2012).
- [91] D. Jordan and P. Smith, *Nonlinear ordinary differential equations: an introduction for scientists and engineers* (OUP Oxford, 2007).
- [92] In the PIC simulations, the work $W_{\parallel,\perp}$ could be recorded on the photon particle. When a photon is emitted from its parent electron, it inherits the work value $W_{\parallel,\perp}$ from the electron at that moment. Therefore, each photon would have an attribute of its parental electron’s work contribution $W_{\parallel,\perp}$. This is convenient for presenting the correlation between the photon polarization and the work contribution (i.e. the acceleration mechanism).
- [93] L. Gremillet, G. Bonnaud, and F. Amiranoff, Filamented transport of laser-generated relativistic electrons penetrating a solid target, *Physics of Plasmas* **9**,

- 941 (2002).
- [94] Y. Sentoku, K. Mima, P. Kaw, and K. Nishikawa, Anomalous resistivity resulting from mev-electron transport in overdense plasma, *Physical Review Letters* **90**, 155001 (2003).
- [95] R. Li, T. Huang, L. Ju, M. Yu, H. Zhang, S. Wu, H. Zhuo, C. Zhou, and S. Ruan, Nanoscale electrostatic modulation of mega-ampere electron current in solid-density plasmas, *Physical Review Letters* **127**, 245002 (2021).
- [96] R. Blandford and D. Eichler, Particle acceleration at astrophysical shocks: A theory of cosmic ray origin, *Physics Reports* **154**, 1 (1987).
- [97] H. Zhang, W. Deng, H. Li, and M. Böttcher, Polarization signatures of relativistic magnetohydrodynamic shocks in the blazar emission region. i. force-free helical magnetic fields, *The Astrophysical Journal* **817**, 63 (2016).
- [98] L. Sironi, I. Plotnikov, J. Nättilä, and A. M. Beloborodov, Coherent electromagnetic emission from relativistic magnetized shocks, *Physical Review Letters* **127**, 035101 (2021).
- [99] R. Duclous, J. G. Kirk, and A. R. Bell, Monte carlo calculations of pair production in high-intensity laser-plasma interactions, *Plasma Physics and Controlled Fusion* **53**, 015009 (2010).
- [100] N. Elkina, A. Fedotov, I. Y. Kostyukov, M. Legkov, N. Narozhny, E. Nerush, and H. Ruhl, Qed cascades induced by circularly polarized laser fields, *Physical Review Special Topics-Accelerators and Beams* **14**, 054401 (2011).
- [101] C. Ridgers, J. G. Kirk, R. Duclous, T. Blackburn, C. Brady, K. Bennett, T. Arber, and A. Bell, Modelling gamma-ray photon emission and pair production in high-intensity laser-matter interactions, *Journal of Computational Physics* **260**, 273 (2014).
- [102] A. Gonoskov, S. Bastrakov, E. Efimenko, A. Ilderton, M. Marklund, I. Meyerov, A. Muraviev, A. Sergeev, I. Surmin, and E. Wallin, Extended particle-in-cell schemes for physics in ultrastrong laser fields: Review and developments, *Physical Review E* **92**, 023305 (2015).
- [103] K. Yokoya and P. Chen, User's manual of cain (2003).
- [104] L. Sironi and A. Spitkovsky, Synthetic spectra from particle-in-cell simulations of relativistic collisionless shocks, *The Astrophysical Journal* **707**, L92 (2009).